# Experimental Study on the Fluorescent Oil-Film Method in Assessing the Impact of Surface Topology on Boundary Layer Separation

Stud. Eng. **Alin Matei POPILIAN**[1,*], Stud. Eng. **Mihai-Alexandru CHIRIȚĂ**[1], Stud. Eng. **Raul SABĂU**[1]

[1] Technical University of Cluj Napoca, 400020, Cluj - Napoca, Romania

* matei.popilian@outlook.com

***Abstract:*** *Due to their shape, spheres possess poor aerodynamic properties, with air separating early, leading to an increase in pressure drag, and thus total drag. By introducing different topologies on the surface, the boundary layer separation can be delayed significantly, which can be correlated with a reduction of the total wake, and consequently with a reduction of both the pressure and the total drag. The present paper presents an experimental qualitative study conducted with the aim of exploring the capacity of the oil film visualization method to assess the aerodynamic effects of surface topology on blunt objects. Three spherical bodies, one with a smooth surface and the others with shallow and deep dimples, all of them coated with a thin layer of fluorescent oil were tested by turn in a low-speed wind tunnel for three values of the airflow's velocities. The flow past each sphere was recorded from two different angles. The resulting images were used to identify the separation points to assess the angle relative to the stagnation point where the flow separates from the surface. Thus, the oil film technique was tested in its capability to identify the boundary layer separation line and to observe its shifting for flows with increasing Reynolds number. Data from literature was used to compare the outcomes and to analyze the separation in case of the flow around the sphere. Overall, this research contributes to a more profound understanding of how the oil-film visualization method can be used to assess the effect of the surface topology on flow separation. The results of this research could also be useful for further research into the broader field of golf ball aerodynamics.*

***Keywords:*** *Golf ball, pressure drag, surface topology, oil film visualization, flow separation*

## 1. Introduction

The spherical shape, with its inherent bluntness, poses significant aerodynamic challenges, especially in applications where drag reduction is crucial. Due to this shape, spheres experience elevated levels of pressure drag, primarily caused by the early separation of the boundary layer along their surface. In the case of smooth spheres, this separation occurs closer to the stagnation point, where the airflow detaches and creates a low-pressure wake at the rear. This separation results in increased drag forces, making spheres inefficient for applications requiring streamlined movement through air or fluid, such as in sports equipment, industrial machinery, and various engineering fields.

Adding certain surface topologies, such as dimples, has been a classic method for addressing these aerodynamic limitations. By incorporating surface dimples, such as those on a golf balls, the transition point from laminar to turbulent flow, can be influenced by shifting the transition point towards the leading edge of the sphere. This shift delays boundary layer separation by increasing the skin friction caused by the turbulent flow over the surface, reducing the low-pressure wake behind the sphere and, subsequently, reducing the overall pressure drag of the body.

Spheres experience four distinct flow regimes, Subcritical, Critical, supercritical and Transcritical. Achenbach 1972 [1] conducted experimentation, on perfectly smooth spheres, to test spherical nuclear fuel cells that are transported at high pressure. The experimentation by Achenbach was conducted in a high pressure tunnel to achieve the high Re values required, achieving all 4 flow regimes. In their experimentation, they found that a sphere is considered in the subcritical flow regime until just under $2x10^5$ Re. After this point, the sphere transitions to the critical Regime between $2x10^5$ and $3.7x10^5$, followed by a supercritical range between $3.7x10^5$ and $1.5x10^6$, and finally the Transcritical Range above $1.5x10^6$.

The dimple, which was adopted in golf in the early 20th century, is significant in inducing a drag crisis towards lower Reynolds numbers. Where the Drag crisis on the smooth sphere occurs at Reynolds numbers of over 200,000, modern dimpled spheres cause this sudden drop in CD at

much lower Reynolds numbers. This reduction of drag coefficient is correlated with an increase in the boundary layer separation angle observed over the surface of the sphere.
There are several other articles related to the boundary layer separation and to the Aerodynamics around blunt objects, that show studies on spheres with different topologies or studies specifically on dimpled spheres, such as those found in golf. Studies range from using different visualization techniques, to quantitative studies using force transducers, to CFD tests.
Results from Achenbach 1974 [2] shows a comparative graph between spheres of different roughness's (k/ds) values, which is a non-dimensional parameter used to define the topology of the sphere in terms of the height of the irregularity and the nominal diameter of the sphere, measured by dividing the dimple depth (k) to the total diameter of the sphere (ds). The roughness elements used were grains of sand pasted on the surface of the sphere; however, it provides good Context as a wide range of k/ds values were provided.
Bearman and Harvey [3] were the first to conduct experiments on golf balls in 1976. They performed both static and spinning tests on scaled up, manufactured golf ball like spheres, with both spherical and hexagonal dimples. Tests were conducted in a closed return type wind tunnel and highlighted some of the key baseline references. The differences between roughness types in [2] and the dimples in golf balls affected the CD value is also noted in the research, determining dimples induce the drag crisis over a larger range of Reynolds numbers.
Newer studies such as those done by J.A. Scobie [4] conducted experimentation using a relatively novel infrared imaging technique, on three types of blunt objects, also manufactured using "rapid prototyping"; smooth, dimpled and that with the geometry of a cricket ball. The Experimentation was conducted at a Reynolds of 100,000 and with a k/ds value of 800x10-5.
A study done by Aoki 2003 [5], who also conducted an experimental study, shows a modern, PIV method, with the assistance of an oil-film visualization technique using a pigment like Titanium Dioxide alongside a liquid paraffin, applied on vinal spheres with dimples, to determine the aerodynamics around, and on the boundary layer, at a Re range between 3x104 and 1.3x105.
Lastly, a study done by N. Beratlis 2019 [6] shows extensive CFD simulation done on golf balls in the subcritical and the supercritical flow regimes. The tests shed light on what occurs inside the dimple of the sphere and how the dimple effects the flow around the surface. CD, CF and separation angles are also noted in their experimentation.
To analyze boundary layer separation and flow characteristics, the oil-film method, developed by NASA in the 1950's [7] was used. This method consists of preparing a thin layer of oil mixed with fluorescent particles that is smeared across the surface of the test model, which is then used to visualize where thickness occurs on the surface due to the shearing action across the boundary layer.
For the smooth spheres, this article covers only the subcritical and part of the critical flow regimes, with a maximum Reynolds of $1.89x10^5$ being achieved. Tests were conducted at three free stream air speeds; 13.4 m/s, 18.78 m/s and 26.8 m/s, using three sphere types, smooth, shallow dimpled and deep dimpled, dimensionally like golf-balls, and scaled up to achieve a diameter (ds) = 105 mm to accurately represent the Reynolds number golf balls travel at.
FDM printing has also brought modern methods of printing that can be used to design and to manufacture prototypes as well as final parts in a fast and efficient way. However, these new manufacturing methods have also brought practical limitations in surface quality and in geometrical tolerancing, leading to relatively high values of roughness across the surface in distinct manners. This effects the way flow is directed over the surface of the sphere, and how the boundary layer separation is affected compared to other manufacturing methods.
The scope of this article is to test the oil-film method itself on FDM 3D printed blunt objects with different topologies, and if this method can and should be used for these 3D printed objects. While focusing on the aspect of additive manufacturing, specifically FDM printing, this article can also have relevance in the wider scope of sphere and golf ball aerodynamics, as well as the study of surface flow visualization techniques.

## 2. Material and Method

### 2.1 Spherical Bodies

Three spheres, with different surface topologies, shown in (Fig.1), were manufactured out of PETG (Polyethylene terephthalate glycol) used for 3d additive manufacturing, with the above mentioned 105mm $d_s$ value, printed using a 0.4 mm nozzle on the Bambu lab x1 carbon 3d printer. The spheres were each the derivative of two hemispheres connected and sealed using a standard transparent plastic glue. The spheres were sanded at the connection point to minimize the effect that the line had with the flow over the surface. The three models evaluated included one with a smooth surface (Fig.1a), one with small-medium sized dimples (Fig1.b), and one with deep dimples (Fig.1c), with sizes comparable to those found on golf-balls. Both dimples were of the spherical type. An experimental support also seen in (Fig.1d) was manufactured using the same material, streamlined to minimise aerodynamic effects due to the support.

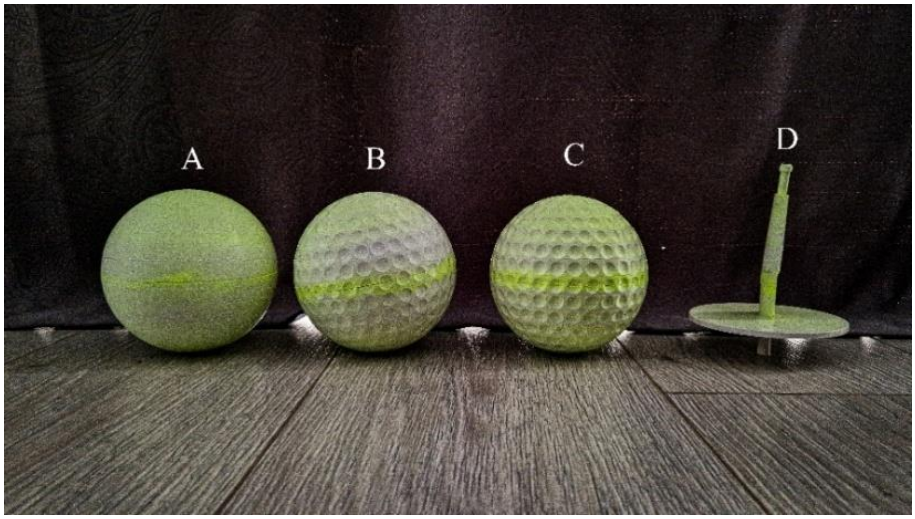


**Fig. 1.** The tested spheres; A (smooth sphere); B (sphere with small-medium sized dimples); C (sphere with deep dimples); and the support used in the experimentation; D (experimental support)

The aerodynamic behavior of spheres is commonly analyzed in connection with the Reynolds number assigned to the flow. The spheres in this study were designed to match Reynolds numbers, and design characteristics of golf balls with spherical dimples. Golf balls commonly have a nominal diameter of 42.7 mm, a dimple depth ($k$) which are measured from the tangent line to the sphere to the bottom of the dimple, measuring between 0.1 to 0.25 mm and have between 300 and 500 dimples, the most common being 328 dimples. The dimples on sphere B and C, were designed to have a similar $k/d_s$ value as commercial golf-ball [8].
These were then scaled up with the scaled diameter, to achieve the correctly scaled parameters. Shown in (Fig.2) is a close of the dimple parameters. The surface roughness of the smooth sphere was measured using the high-performance roughness measuring device TR220/TIME3202 that has a measuring range between Rz=0.02-160 μm, where Rz value, measured in micrometers, is the average between the maximum and the minimum peaks on the surface of five consecutive sampling lengths. An inspection system, Axiom too CMM from Aberlink was used to measure the circularity High spec shop floor CMM, which read a Rz value for the smooth sphere of 9.378 μm.

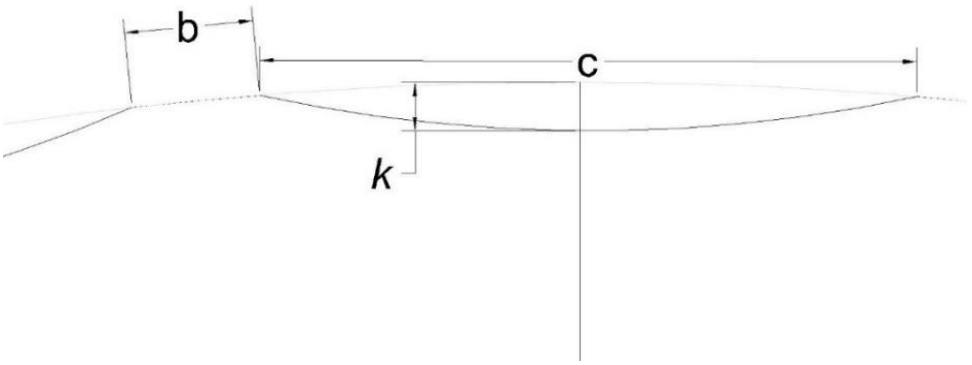


**Fig. 2.** Close up of the dimple parameters

The dimple depth (*k*), the diameter of the dimple (c) the nominal diameter ($d_s$) as well as the real diameter, ($d_{sR}$) the number of dimples ($n_{dim}$), the relative roughness of the dimples ($k/d_s$), the roughness of the smooth sphere (Rz) and the circularity tolerance (Cir), measured using a High spec shop floor CMM, Axiom too CMM from Aberlink, are all highlighted below in (Table 1.).

**Table 1:** Sphere Specifications

| | $d_s$ [mm] | $d_{sR}$ | *k* [mm] | c [mm] | $n_{dim}$ | $k/d_s$ [$10^{-5}$] | Rz [µm] | Cir [mm] |
|---|---|---|---|---|---|---|---|---|
| Sphere A | 105 | 104.53 | - | - | - | - | 9.378 | 0.233 |
| Sphere B | | 104.48 | 0.254 | 8.61 | 328 | 242 | - | 0.102 |
| Sphere C | | 104.38 | 0.635 | | | 605 | - | 0.107 |

The speed that these golf balls can travel at varies greatly based on the skill of the golfer. Average golfers can achieve golf ball speeds of 43.7 m/s, approximately 154 km/h, which, under standard conditions, gives a Re value of approximately $1.3x10^5$. Professional golfers on the other hand, can achieve hits with velocities ranging from 63 m/s to 72 m/s average (227-260 km/h), which gives a Re from approximately $1.8x10^5$ to $2.07x10^5$ [9]. Considering this, as well as a known maximum wind tunnel velocity of 26.8 m/s, the spheres tested were scaled up to a diameter of 105mm to achieve the targeted Reynolds number. As well, Reynolds number calculations were based on atmospheric conditions in Cluj-Napoca, Romania, with an air density $\rho_1$ of 1.214kg/m³, calculated for an ambient temperature of 18°C with an air pressure of 1015.1 mb [10]. Using Sutherlands law under standard conditions [11] for air at 18°C, the dynamic viscosity of air under these conditions is found to be $1.803 \times 10^{-5}$ Pa·s Considering the above values for dynamic viscosity and for density, and the tested $d_s$ value, there are three Reynolds numbers calculated for 3 utilized test speeds; $9.47x10^5$ at 13.4 m/s velocity; $1.33x10^5$ at 18.78 m/s; $1.89x10^5$ at 26.8 m/s.

### 2.2 Oil Film Mixture

The oil mixture used in the experiment was a 2:1 mix of R-134A florescent oil (56 ml when tested) produced by Elke, and a universal paint thinner (28 ml when tested). This mixture was measured before experimentation using a DV2T Rotational Viscometer, using an x/y cylinder system, run for a duration of 10 minutes, and was determined to have a dynamic viscosity of 8.88 cP +- 0.15 cP. The density was calculated using a simple mass volume calculation, with a density found to be 1.13 kg/m³. Lastly, the kinematic viscosity was calculated, giving us a value of 7.87 mm²/s. While the density and the viscosities are highly relevant for the ease of visualization with different wind tunnel speeds, in conformity with A.Terzis [12] or for calculating the skin friction forces using the oil-film method [13], the scope of the article was only to visualize the boundary layer separation and some details regarding the boundary layer conditions. For this reason, the viscosity of the oil

was not of the highest relevance due to it being independent of the oil pattern formed as explained in R. L. Maltby 1962 [14]. The aimed for viscosity of 9 cP was therefore chosen due to factors regarding the ease of visualization at the low Reynolds numbers covered in this article.

### 2.3 Experimental Setup

All experimentation was conducted in the UTCN low-speed wind tunnel, shown in a sketch done from the lateral view in (Fig.3), manufactured by the company Sangari for UTCN.

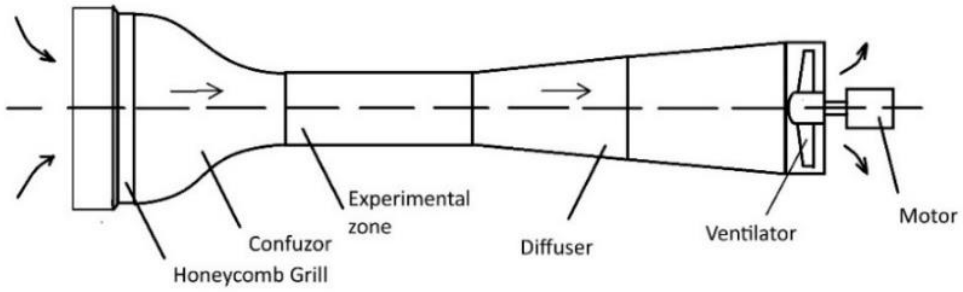


**Fig. 3.** Sketch of the UTCN low speed wind tunnel

In the tunnel, the maximum flow velocity that could be reached was 26.8 m/s. The tunnel testing zone has a square cross-section of 250 mm by 250 mm, and a length of 750 mm. The placement of the phone's camera and the UV flashlight differ from the top and side tests, as seen in (Fig.4).

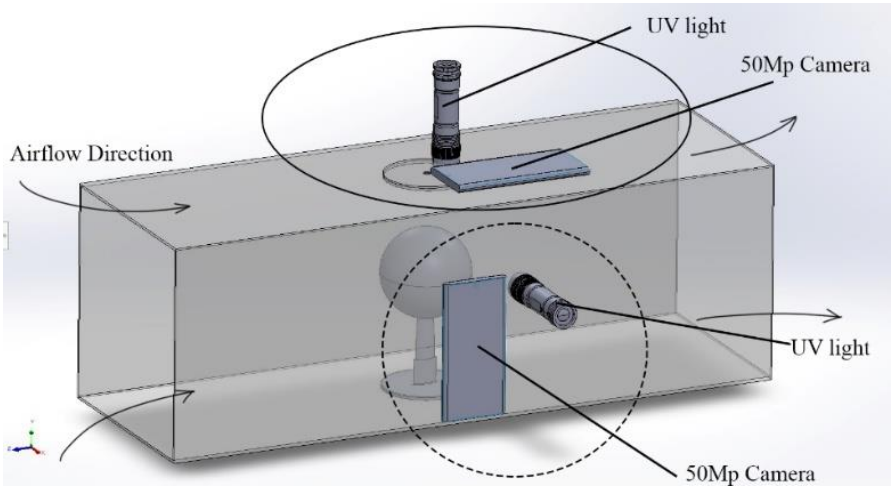


**Fig. 4.** Visual representation of the testing zone together with the position of the 50 Mp camera and flashlight at the "Top View" position marked with a solid line and "Side View" position marked with a dashed line

The sphere support was mounted inside the test section using a tight fit, mounted with its elongated profile towards the airflow, attached with one of the three spheres to be tested. The sphere assembly was then placed into the experimentation section using the 8 mm hole at the bottom of the tunnel as a guide. A camera with the specification of 50Mp, was placed in the "side view" position, see (Fig.4), alongside a standard UV light with a $\lambda$ value of 395nm. Shown in (Fig.5) is a close-up of the experimental setup.

**Fig. 5.** Close up to the test section prior to experimentation on Sphere A upwind and to an angle

### 2.4 Methodology

All experimentation was done in a dark room, and the experiment was run. For each experiment, the spheres were coated with a uniform layer of fluorescent oil mixture. There were three experiments done, one using the oil film method from the "side view," one using the oil film method form the "top view". For the experimentation done using the oil-film method, the wind tunnel was then run at 3 different free stream velocities, one for a speed of 13.4 m/s, one for a speed of 18.78 m/s and one for a speed of 26.8 m/s for two to five minutes each with a camera running, repeated for spheres A, B and C. Observations were made by examining the position and pattern of the flow separation line on the sphere's surface and the time taken to achieve saturation at the separation point. The experiment was the repeated, however this time using the filming position "top view" to visualize the separation point. The spheres were then wiped, and the camera and UV light was placed back in the "side view" Position. All experimentation was then repeated on spheres A, B and C in the same experimental conditions. Observations were made by analysing the captured videos frame by frame and taken from the first points in which flow separation is determined. The images were then processed, and the position and pattern of the flow separation line on the sphere's surface were determined using computer software. The error was then calculated to determine the feasibility of the method in a wider context. The software that was used provided marking lines that were used to determine two principal distances; a, the total distance between the stagnation point and the most rearward point on the sphere compared to the airflow, and b, the distance between the separation points and the stagnation point. The total distance as well as the three points taken are shown in (Fig.6), where the software's ruler software is shown by a dotted line, where the arrows show where on the sphere the three points of separation was taken.

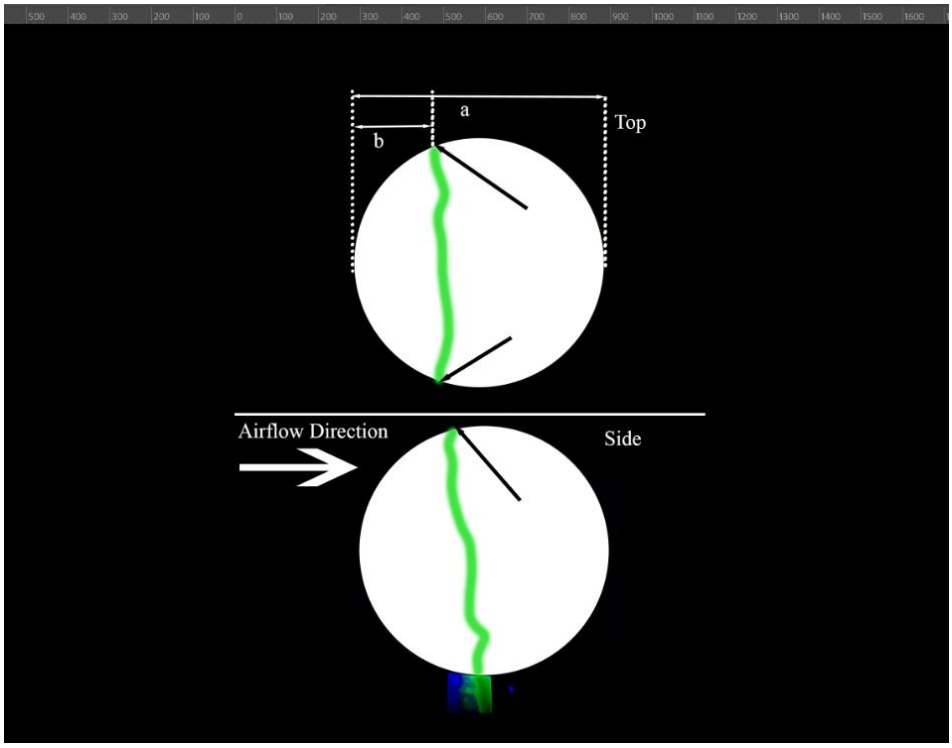


**Fig. 6.** Identifying the separation points on the boundary layer separation line(sketch)

The image was magnified to the pixel level onto the edge of the separation line where the section of the sphere is located, and the value between the stagnation point and the point chosen was taken. These values were then plugged into a CAD software to determine the angle formed when the distance from the stagnation point to the line was at the distance shown. This angular position of the separation points which was assessed from the images using visual analysis, is taken as shown below in (Fig.7), the same as how other studies [1-3] have taken the position.

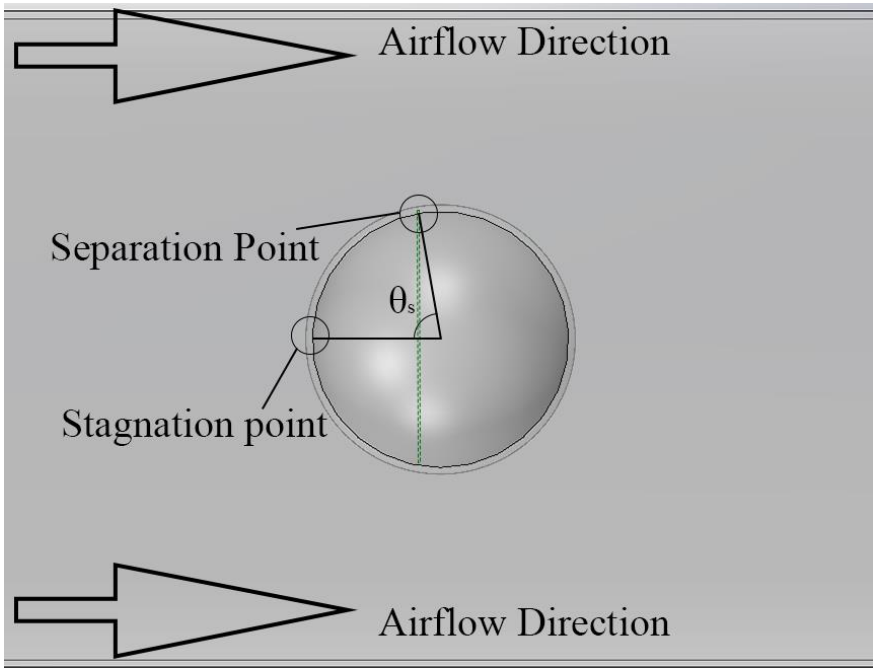


**Fig. 7.** Angle of separation from the stagnation point to the separation point

The Error rate was then determined by a variety of factors such as the effect the oil has on the airflow, the lighting and the Camera factors, as well as the deviation between the values at the three points taken. The oil error has on boundary layer separation is taken from Maltby 1962 [13] which states "Thus in general the oil will only have a small influence on the boundary layer, changing the distance to separation by at most 2%". This 2% error can be factored in by adding the 2% to the angle of separation observed. The Effects that lighting and camera had on the experimentation were determined from the gradient of the oil separation line and the distance between where pixels start to become dark to the point that shows a clear, dark contrasted pixel. This was taken using the context of the wider image as well due to the issues regarding lighting. This is shown below in (Fig.8) as the example that was taken to determine the error which came out to be 1% for sphere A. The error was also taken for sphere B and C and was determined to be a total of 4% .Lastly the error occurring due to the deviation between the three values taken from the top view (2 points) and the side view (1 point) was simply taken as a simple min/max limit which was factored in by taking the average of the three values.

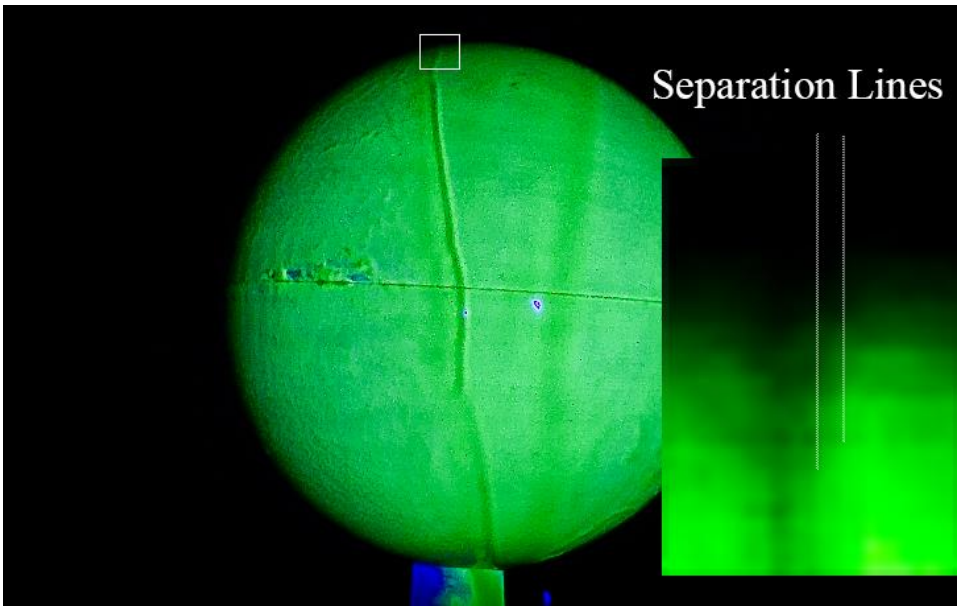


**Fig. 8.** Zoomed in image of sphere A, at a Re = $1.33x10^5$, showing the separation line at the pixel level

## 3. Results and Discussion

### 3.1 Visualization study sphere A

The experimentation on sphere A (smooth) using the Oil film method, was filmed from the top view as shown in (Fig.9a), (Fig.9c) and (Fig.9e), as well as the side view as shown in (Fig.9b), (Fig.9d) and (Fig.9f). Focusing on the first Reynolds number tested at $9.47x10^5$ in (Fig.9a) and (Fig.9b), a distinct saturation of oil is observed on the surface of the sphere. The boundary layer separation line was determined to occur at 80° from the side view and at 78° and at 79° from the Top view. Accounting for the 2% error due to the interference with oil, the angle increases an angle of 82°, 80° and 81° respectively for all three points. The average of the three values is determined to be 81°. This is similar with research done by [1,4,5]. Also observed are some distinct surface features towards the leading edge in (Fig.9b), caused by some small turbulences due to the imperfect surface of the 3D printed material, as well as slight disturbances in the saturation line. Moving onto (Fig.9c) and (Fig.9d), which had a Re of $1.33x10^5$, there is an observed and distinct, thin, thickness in the oil is observed on the surface of the sphere. The boundary layer separation line was determined to occur at 80° from the side view and at 81° from the Top view. Accounting for the 2% error due to the interference with the oil, the position of the angle increases to 82°, 83° and 83° respectively. The average of the three values is determined to be 83°. This is a bit higher than the results found to the values found by Achenbach 1972[1], most probably due to the higher tunnel

speed being able to move more oil towards the real point of separation, negating the error correction done somewhat. Another observation can be made in that there is a barely visible line towards the trailing edge of the sphere in (Fig.9d). This was caused by heavy turbulence, most likely caused by increased air recirculation at higher speed. While the flow regime is still considered subcritical, the support on the lower part of the sphere could contribute to a change from laminar to turbulent on the lower end of the sphere earlier than expected.

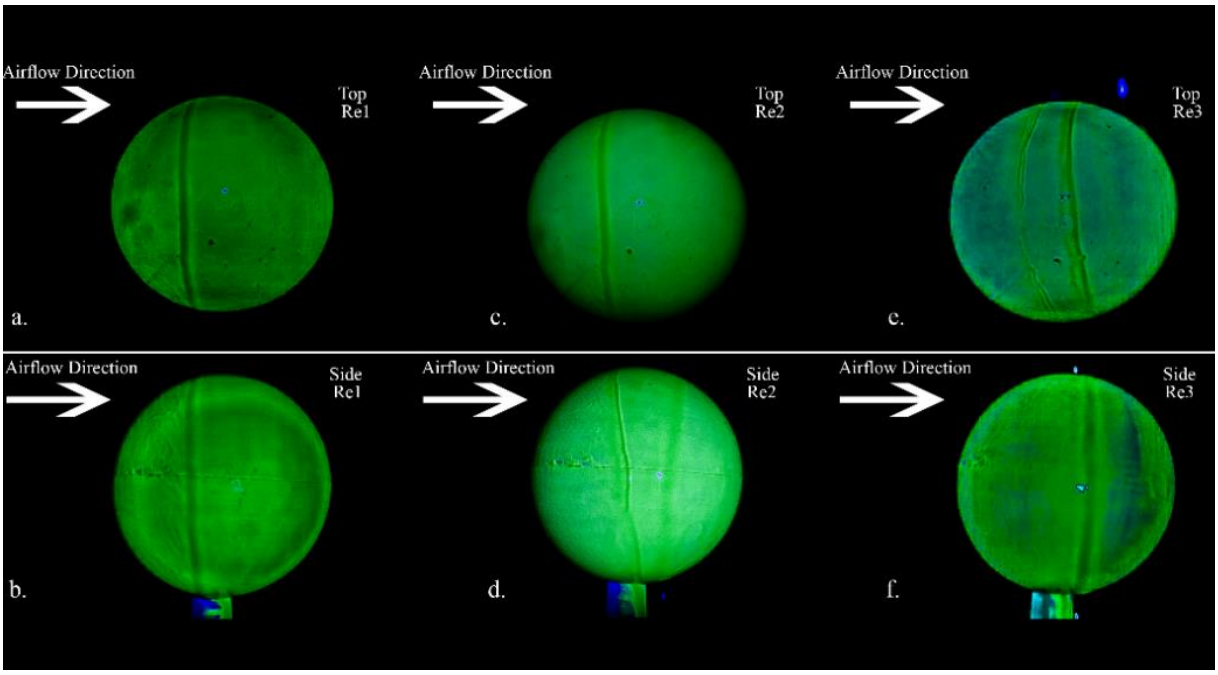


**Fig. 9.** Test sphere A at different angles and speeds; a) Top view at Re = $9.47x10^5$; b) side view at Re = $9.47x10^5$; c) Top view at Re = $1.33x10^5$ ; d) side view at Re = $1.33x10^5$; e) Top view at Re = $1.89x10^5$ ; f) side view at Re = $1.89x10^5$

Lastly, in (Fig.9e) and (Fig.9f), which were tested at a Re of $1.89x10^5$, the position of the boundary layer separation changes drastically towards a higher $\theta_s$ value compared to the lower Reynolds numbers. The boundary layer separation line was determined to occur at 104° from the side view and at 98° and 102° from the Top view. Again, accounting for the 2% error due to the interference with the oil, the position of the angle increases to 106°, 99° and 103° respectively. The average of the three values is determined to be 103°. When compared to articles [2,3], the observed separation only starts to increase at the Re value of $1.9x10^5$ and observed separation at 97° at a value close to $2.5x10^5$ Re, the boundary layer separation seems to increase in angle prematurely. This is most likely caused by the roughness value on Sphere A, as well as the imperfections in the geometry of the sphere itself. Another observation in (Fig.9e) is the additional line in front of the boundary layer separation line. This can be attributed most likely to the transition from laminar to turbulent flow over the surface. Lastly, there is a clear drop in the precision of the values at Re = $1.89x10^5$ compared to the lower Re values. This most likely is attributed to the regime of flow around the sphere going from subcritical to critical, disturbing the flow patterns more heavily than the steady, fully laminar flow around the sphere in the first two cases.

### 3.2 Visualization study sphere B

The experimentation on sphere B ($k/d_s$ = 242) using the Oil film method, was filmed from the top view as shown in (Fig.10a), (Fig.10c) and (Fig.10e), as well as the side view as shown in (Fig.10b), (Fig.10d) and (Fig.10f). The first tests of Re = $9.47x10^5$ shown in (Fig.10a) and (Fig.10b), show difficult to read values of separation. The boundary layer separation line was determined to occur at 106° from the side view and at 105° and 107° from the Top view. Accounting for the 2% error due to the interference with oil, the angle increases an angle of 108°, 107° and 109° respectively. The average of the three values is determined to be 108° with the 2% error accounted for.

Observed in (Fig.10a) and (Fig.10b), are streaks and markings showing boundary layer separation. The way the oil clumps up inside the dimple should also be noted as being weak and in random directions to the airflow in some areas.

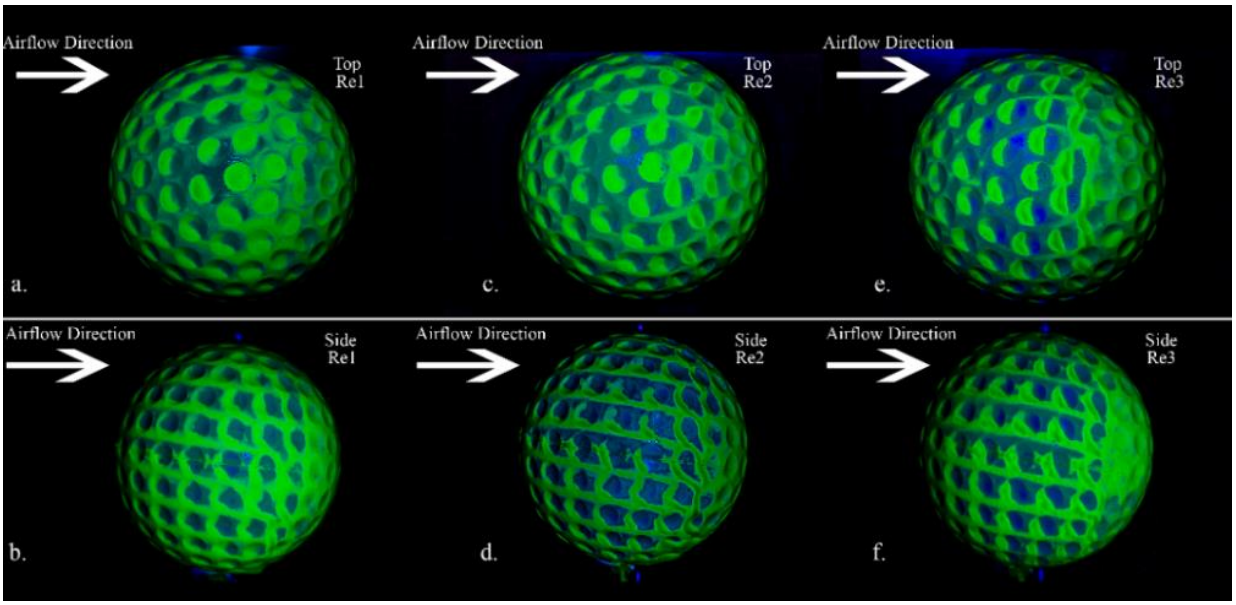


**Fig. 10.** Test sphere B at different angles and speeds; a) Top view at Re = 9.47x10$^5$; b) side view at Re = 9.47x10$^5$; c) Top view at Re = 1.33x10$^5$ ; d) side view at Re = 1.33x10$^5$; e) Top view at Re = 1.89x10$^5$ ; f) side view at Re = 1.89x10$^5$

With the increased tunnel speed in (Fig.10c) and (Fig.10d), which had a Re of 1.33 x10$^5$, there is an observed increase in the distinction of the oil pattern, as well as a further delay in separation. The boundary layer separation line was determined to occur at 114° from the side view and at 114° and 118° from the Top view. Accounting for the 2% error due to the interference with the oil, the position of the angle increases to 116°, 116° and 120° respectively. The average of the three values is determined to be 118° with the 2% error accounted for. This is a reasonable prediction according to data from scobie [4]. The way oil clumps inside the oil also increases in intensity, keeping the same pattern directions. Further increases in the tunnel speed, shown in (Fig.10e) and (Fig.10f), which were tested at a Re of 1.89x10$^5$, does not influence the position of the boundary layer, which remains at the same angle compared to the lower Reynolds numbers tested. The boundary layer separation line was determined to occur at 114° from the side view and at 116° and 117° from the Top view. Again, accounting for the 2% error due to the interference with the oil, the position of the angle increases to 116°, 118° and 119° respectively. The average of the three values is determined to be 118° with the error accounted for. This is most likely due to the critical Reynolds number being achieved before this point, allowing the sphere to most likely enter the supercritical flow regime.

### 3.3 Visualization study sphere C

The experimentation on sphere C ($k/d_s$ = 605) using the Oil film method, was filmed from the top view as shown in (Fig.11a), (Fig.11c) and (Fig.11e), as well as the side view as shown in (Fig.11b), (Fig.11d) and (Fig.11f). At a Re = 9.47x10$^5$ shown in (Fig.11a) and (Fig.11b), the results seem to be of similar quality to that of sphere C. However, through closer analysis, the oil smear can be observed just as easily as Re values that were higher on Sphere b. The boundary layer separation line was determined to occur at 114° from the side view and at 118° and 116°from the Top view. Accounting for the 2% error due to the interference with oil, the angle increases an angle of 116°, 120° and 116° respectively. The average of the three values is determined to be 118° with the 2% error accounted for. The results appear to agree to the data from [3] which indicated, for a golf ball of $k/d_s$ = 900, that the critical Reynolds number would be around 6x10$^4$. This could indicate that the Critical Reynolds number of sphere C, with a $k/d_s$ = 605, could be in between 6x10$^4$ and 9x10$^4$. The

angle of 119° is also considered to be common for golf balls at that Reynolds. [4], for example, indicates a separation angle of 120° at a Reynolds of $1x10^5$. It should also be noted that the oil inside the dimples seems to be trending towards the airflow, and down, the latter effect most likely caused by gravity. Results obtained at a Re = 1.33 $x10^5$, show in (Fig.11c) and (Fig.11d), shows the observed angle drops instead of staying at 120°. While the line is not distinct, the smearing across the surface where there is a clear difference of oil is taken. The boundary layer separation line is determined to occur at 109° from the side view and at 115° and 115° from the Top view. Accounting for the 2% error due to the interference with the oil, the position of the angle increases to 111°, 117° and 117° respectively. The average of the three values is determined to be 115° with the 2% error accounted for. This high reduction in angle is most probably caused by the surface imperfections caused by printing, as well as the tendency for a gradual increase in CD value in the supercritical phase of a golf ball. [2] observed greater changes in CD, and thus separation angle than [3] due primarily to the use of external roughness instead of dimples. Less oil buildup is observed inside the dimples; however, it is noticed that the general trend mentioned previously is still valid.

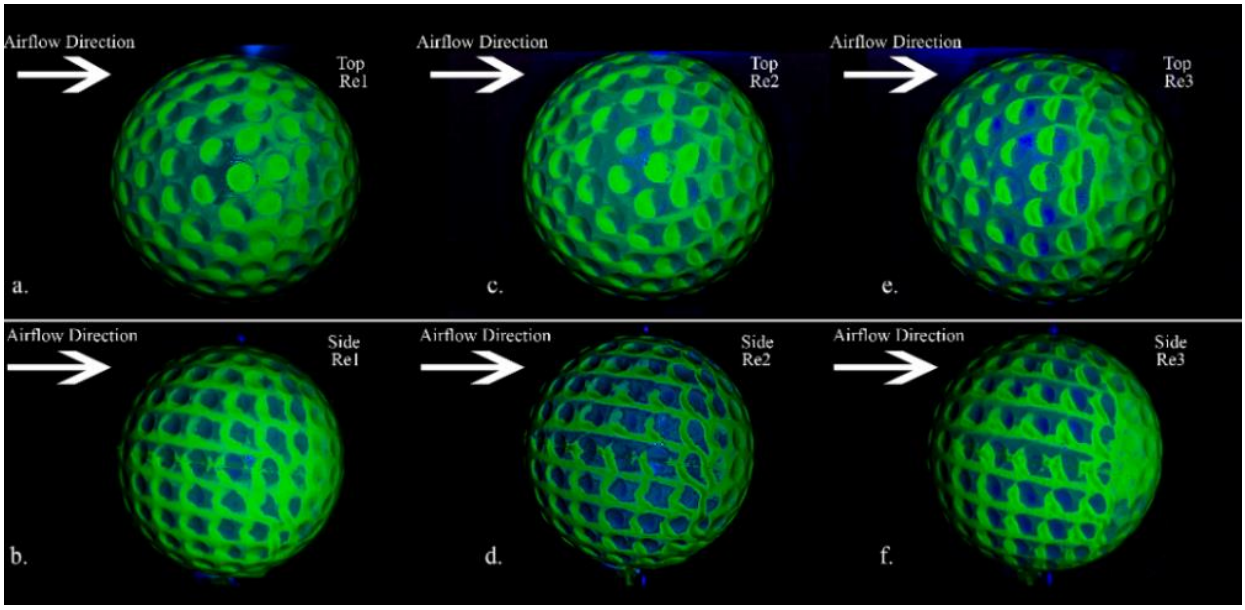


**Fig. 11.** Test sphere C at different angles and speeds; a) Top view at Re = $9.47x10^5$; b) side view at Re = $9.47x10^5$; c) Top view at Re = $1.33x10^5$ ; d) side view at Re = $1.33x10^5$; e) Top view at Re = $1.89x10^5$ ; f) side view at Re = $1.89x10^5$

The further increase in tunnel speed, shown in (Fig.11e) and (Fig.11f), which were tested at a Re of $1.89x10^5$ shows the position of the boundary layer separation changes towards an even lower $\theta_s$ value. The boundary layer separation line was determined to occur at 106° from the side view and at 109° and 115° from the Top view. Again, accounting for the 2% error due to the interference with the oil, the position of the angle increases to 108°, 111° and 117° respectively. The average of the three values is determined to be 112° with the error accounted for. This further drop in angle indicates the same phenomenon as indicated above regarding the surface roughness effects on the change of angle.

### 3.4 Overall Results

The results were taken and placed in two different tables, separating values without any correction in the error due to the oil-film interference (Table 2.), and with the 2% error (Table 3.). This is done to provide a context of the values taken pixel by pixel, and what separation is calculated to be.

**Table 2:** Results oil film method without error correction

| | Sphere | Reynolds Number | Separation point | | | |
|---|---|---|---|---|---|---|
| | | | Side view | Top view | | Average |
| | | | Angle (1) $\theta_s$[°] | Angle (2) $\theta_s$[°] | Angle (3) $\theta_s$[°] | Angle (1-3) $\theta_s$[°] |
| Experiment I | A | $9.47x10^5$ | 78 | 79 | 80 | 79 |
| | | $1.33 x10^5$ | 81 | 81 | 80 | 81 |
| | | $1.89x10^5$ | 103 | 99 | 106 | 103 |
| Experiment II | B | $9.47x10^5$ | 107 | 105 | 106 | 106 |
| | | $1.33 x10^5$ | 118 | 114 | 114 | 115 |
| | | $1.89x10^5$ | 116 | 117 | 114 | 116 |
| Experiment III | C | $9.47x10^5$ | 118 | 116 | 114 | 116 |
| | | $1.33 x10^5$ | 115 | 115 | 109 | 113 |
| | | $1.89x10^5$ | 109 | 115 | 106 | 110 |

**Table 3:** Results oil film method with error correction

| | Sphere | Reynolds Number | Separation point | | | |
|---|---|---|---|---|---|---|
| | | | Side view | Top view | | Average |
| | | | Angle (1) $\theta_s$[°] | Angle (2) $\theta_s$[°] | Angle (3) $\theta_s$[°] | Angle(1-3) $\theta_s$[°] |
| Experiment I | A | $9.47x10^5$ | 80 | 81 | 82 | 81 |
| | | $1.33 x10^5$ | 83 | 83 | 82 | 82 |
| | | $1.89x10^5$ | 105 | 101 | 108 | 105 |
| Experiment II | B | $9.47x10^5$ | 109 | 107 | 108 | 108 |
| | | $1.33 x10^5$ | 120 | 116 | 116 | 118 |
| | | $1.89x10^5$ | 118 | 119 | 116 | 118 |
| Experiment III | C | $9.47x10^5$ | 120 | 118 | 116 | 118 |
| | | $1.33 x10^5$ | 117 | 117 | 111 | 115 |
| | | $1.89x10^5$ | 111 | 117 | 108 | 112 |

The chart plotted in (Fig.12), shows three distinct lines showing the $\theta_s$ angle, with correction, plotted against Reynolds number. The first evident trend in the results is the much larger difference in separation line between the smooth and the dimpled spheres. This was to be expected and validates the known fact that the dimples induce separation. The second observation is the difference between where the separation point begins to rise on the smooth sphere in Achenbach 1972 [1] and Sphere A. While the beginning of the rise cannot be pinpointed exactly, it is known that sphere A experiences an angle of 103° at $1.9x10^5$, the same angle is estimated to occur at just over $3x10^5$ in [1]. This is most likely caused by the surface roughness, Rz = 9.378 μm. However, the general trend of sphere A is in good agreement with those found in [1].

Achenbach 1974 [2], Bearman and Harvey [3], Scobiea [4] Aoki [5] and N. Beratlis [6] were used to compare the results for spheres B and C. [2] contained multiple results across various Reynolds, and various roughness's. However, it is difficult to compare results due to the difference in the roughness pattern being grains of sand vs dimples. [3] was used due to their comparison between the CD values of [2] and their own. Due to CD being correlated with the separation angle, parallels can be made between those results. [4] is used to validate some results, however due to having only one result at only one Reynolds, and using one type of golf ball, it is difficult to validate the trends. [5] provides data on separation angles as well, however the dimples used were deep, and the method of determining the separation angle is not clear. Lastly [6] provided CFD testing to

validate separation angle, determining global separation to occur at around 110°. Sphere B provides its peak value, at an angle just above 118° between 1.3x105 and 1.9x105. This is confirmed through [4], obtaining results between 110° and 120° at 100,000 Re and [6]. This also indicates the critical Reynolds number is between those two Reynolds numbers. Any increase in Reynolds number past this is most likely supercritical. Observed on sphere C is the gradual decrease in the separation angle from 118°.Seen in [3] in Figure 1, once the golf ball has achieved its critical Reynolds number, there is a gradual increase in the CD value which is correlated with separation angle. However, the rate at which sphere C's angle decreases is high. This could be because of the roughness and imperfection in the geometry due to 3D printing causes. Due to the decrease in the separation angle occurring throughout all three tests, it can be assumed the critical Reynolds number for sphere C occurs before 100,000 Re.

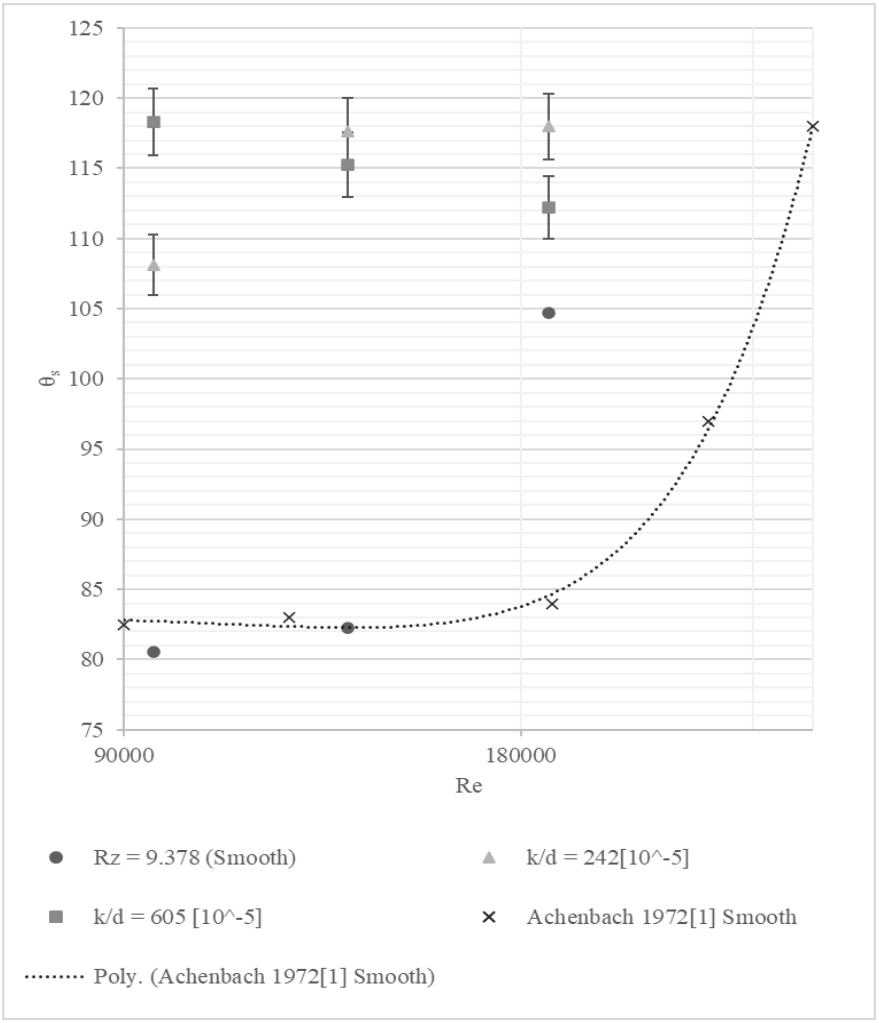


**Fig. 12.** Comparison chart of the separation angles $\theta_s$ with the 2% correction, taken from the stagnation point to the separation point, plotted against the Reynolds Number, compared to data plotted from data taken from Achenbach 1974 [1]

The tolerances on the spheres were taken for the better understanding of error found in the experimentation. These errors were most probably caused by the material that was taken off during sanding, the thermal warping (minimized due to the material used) as well as the 3D printer's tolerance value. As an effect of these issues, the sphere diameter changes from $d_s$ to $d_{sR}$. Recalculating the Reynolds number, the value of 188,618 is calculated at a speed of 26.8 m/s, which is found to have a 0.45% error in Reynolds value compared to the original value of 189,473. This is done for sphere A. The errors in sphere B and C are 0.5% and 0.59% respectively. Considering the measured roughness and the small error in circularity, the critical Reynolds

number may be slightly lower than the previous results by a small percentage, however not by enough to be considered significant.

### 3.5 Future work

Further improvements could include higher resolution cameras, to capture pixels with smaller sizes, allowing for the more precise measuring of the points. further Improved lighting, for example the inclusion of more luminosity, however less intense lighting, to capture the entirety of the sphere, could help in reducing errors due to the darkening of some sections. PIV Experimental Investigations as shown in [15] could be used to increase accuracy and to validate the findings of the oil film method as well. An improved support, such as the one used in Achenbach 1972[1], by Aoki [5], who used a piano wire or by Bacon and Reid 1924 [16], which uses a support that is attached to the rear of the sphere, could reduce errors induced by the support. A change of oil viscosity should also be implemented depending on the speed the tunnel is run at, as to reduce the amount of oil remaining on the entire surface of the sphere. Different manufacturing methods should also be used for a higher accuracy of the results, to improve the roughness on the surface, as well as to decrease geometrical errors. Lastly, implementing more result points, at a wider range of surface speeds, would help in increasing the precision and the accuracy of the trend lines.

## 4. Conclusions

This study confirms the potential and feasibility of using the oil-film visualization method in the determination of boundary layer separation and possibility boundary layer conditions on 3D printed spherical objects with different topology. While there are some limitations of this method, such as the effect the oil has on the distance of the separation line, as well as the inherent issues regarding visualization techniques, such as human error, and the limitations of camera and lighting equipment. However, with all the limitations, it has the potential to provide a large set of data results, with relatively low effort.

Alongside the principal scope of the article, there were other key points that could be determined. Firstly, the roughness on the surface of the sphere heavily impacts the boundary layer conditions and could possibly even be used to good effect to create more turbulence caused by the roughness itself. Secondly, the flow inside the dimples of the sphere could be noticed in some regards, giving a good indicator of how boundary layer is affected inside the dimples.

Future work could include the measurement of different textures on spheres, or with different geometries for topologies and trips. This work could be improved as well to include changes in oil viscosity, better equipment, as well as more accurate camera equipment. Tests can be conducted using oil film visualization techniques to determine flow at the boundary layer with added spin.

**Acknowledgments**

This work was done with financial support and 3D printed materials with the help of AIMA Innovations SRL. The support of. Florin Bode is also noted in providing general support in the writing of the article. The support of Conf. Grigore Marian Pop is also noted in the measurement of tolerancing for the three example spheres. Daniel Banyai provided expertise in the interpretation of the results, verified all the results that were taken correctly, and coordinated the project. Corina Maria-Giurgea provided the support with the writing of the article, the analysis of all information, and coordinated the project. Alin Matei Popilian was responsible for the project organization, the conception of the work, the design and the chosen experimentational conditions, the collection of data from the wind tunnel, the interpretation and analysis of the results, as well as the writing and most of the research for this paper. Mihai-Alexandru Chiriță collected and analysed data from the wind tunnel and worked on the design of the dimpled spheres. Raul Sabău collected and analysed data from the wind tunnel.

**References**

[1] Achenbach, E. "Experiments on the flow past spheres at very high Reynolds numbers." *Journal of Fluid Mechanics* 54, no. 3 (1972): 565-575. https://doi.org/10.1017/S0022112072000874.

[2] Achenbach, E. "The effects of surface roughness and tunnel blockage on the flow past spheres." *Journal of Fluid Mechanics* 65**,** no. 1 (1974): 113–125. https://doi.org/10.1017/S0022112074001285.

[3] Bearman, P.W., and J.K. Harvey. "Golf Ball Aerodynamics." *Aeronautical Quarterly* 27, no. 2 (1976): 112–122. https://doi.org/10.1017/S0001925900007617.
[4] Scobie, J.A., C.M. Sangan, and G.D. Lock. "Flow Visualisation Experiments on Sports Balls." *Procedia Engineering* 72 (2014): 738–743.
[5] Aoki, K., A. Ohike, K. Yamaguchi, and Y. Nakayama. "Flying Characteristics and Flow Pattern of a Sphere with Dimples." *Journal of Visualization* 6 (2003): 67-76.
[6] Beratlis, N., E. Balaras, and K. Squires. "On the origin of the drag force on dimpled spheres." *Journal of Fluid Mechanics* 879 (2019): 147-167. https://doi.org/10.1017/jfm.2019.647.
[7] Loving, D.L., and S. Katzoff. "The fluorescent-oil film method and other techniques for boundary-layer flow visualization." NASA Memorandum 3-17-59L, Langley Research Center (1959).
[8] World Weather Online. "Cluj-Napoca Annual Weather Averages." Accessed November 13, 2025. https://www.worldweatheronline.com/cluj-napoca-weather-averages/cluj/ro.aspx#:~:text=Average%20Pressure%20(mb)%20Graph%20for%20Cluj%2DNapoca&text=Range%3A%201014%20to%201020
[9] COMSOL website. Accessed October 13, 2025. https://doc.comsol.com/5.5/doc/com.comsol.help.cfd/cfd_ug_fluidflow_high_mach.08.27.html.
[10] Medium.com. "How Fast Does the Average Golf Ball Travel?" The golf hype. Accessed October 13, 2025. https://medium.com/@thegolfhype.com/how-fast-does-the-average-golf-ball-travel-17edc632e10e.
[11] Cunningham, Kevin. "How many dimples on a golf ball?", March 18, 2019. EB Golf Media LLC website. Accessed November 12, 2025. https://golf.com/gear/golf-balls/how-many-dimples-on-a-golf-ball/?srsltid=AfmBOooVcrubRJV1HuU9IcejCYyN_JmcmWDxSf2-mtgNU47mzlECa5D3.
[12] The Engineering ToolBox. "Thermodynamic properties of refrigerant R-134a", engineeringtoolbox.com website. Accessed November 12, 2025. https://www.engineeringtoolbox.com/r134a-properties-d_1682.html.
[13] Terzis, Alexandros, Pavlos K. Zachos, Bernard A. Charnley, and Anestis I. Kalfas. "Application of oil and dye flow visualization in incompressible turbomachinery flows." Paper presented at the XXV Biennial Symposium on Measuring Techniques in Turbomachinery (MTT 2020), Santorini, Greece, September 21-23, 2020. *E3S Web of Conferences* 345 (2022): 02003. https://doi.org/10.1051/e3sconf/202234502003.
[14] Maltby, R. L., and R. F. A. Keating. "The Surface Oil Flow Technique for Use in Low Speed Wind Tunnels." In *AGARDograph*, document AGARD-70 (1962): 17, 22-23.
[15] Giurgea, C., F. Bode, L. Nascutiu, D. Banyai, and L. Marcu. "On investigating the flow through an axisymmetric channel with sudden changes in geometry." Paper presented at the 7th International Conference "Experimental Fluid Mechanics 2012" (EFM12), Hradec Králové, Czech Republic, November 20–23, 2012. *EPJ Web of Conferences* 45 (2013): 01119. https://doi.org/10.1051/epjconf/20134501119.
[16] Bacon, D.L., and E.G. Read. "The resistance of spheres in wind tunnels and air." National Advisory Committee for Aeronautics (NACA). Langley Memorial Aeronautical Laboratory. Report No. 185. Washington Government Printing Office, 1924.